To be presented at the Ceramic Materials Symposium at the International Mechanical Engineering Congress and Exposition Winter Annual Meeting of the ASME, Nov. 11-16, 2001, New York Hilton and Towers, NY.

Piezoelectric Materials for an Artificial Neural System

M. J. Schulz
NSF Center for Advanced Materials and Smart Structures
Department of Mechanical Engineering
University of Cincinnati, Cincinnati, OH 45221

S. Chattopadhyay, M. J. Sundaresan, A. Ghoshal, W. N. Martin
NSF Center for Advanced Materials and Smart Structures
Department of Mechanical Engineering
North Carolina A&T State University, Greensboro, NC 27411

P. R. Pratap
Department of Physics and Astronomy
University of North Carolina at Greensboro
P.O. Box 26170, Greensboro, NC 27402-6170

ABSTRACT

Piezoelectric materials are opening the door for the design of large smart structures. To explore what possibilities there might be for building practical smart structures, a review of the characteristics and methods of processing piezoelectric active materials is given. The advantages and limitations of using the different forms of piezoelectric materials for sensors and actuators are then discussed. One area where piezoceramic sensors can have a large impact is structural condition monitoring. Structural condition monitoring refers to using in-situ sensors to monitor the internal loads and the health of a structure in real-time. This will allow a structure to be operated at its maximum performance and efficiency while minimizing the fatigue damage. To achieve this on a large structure, a new highly distributed sensor concept is discussed in which piezoceramic ribbon fibers and microelectronic components are used to replicate the biological nervous system. A simplified simulation and experiment are then presented to show how this artificial neural system can measure dynamic strains and acoustic emissions caused by damage in structures.

Keywords: Piezoelectric Fiber, Structural Condition Monitoring, Artificial Neural System

1. INTRODUCTION

The scientific objective of smart structures research is to develop analogic synthetic bionic structures that will sense, react, and adapt to their environments, and self-monitor their condition to prevent degradation. The socio-economic benefit of this research will be ubiquitous, and it will help to extend the reach of mankind to other planets. The intent of this paper is to discuss how piezoelectric materials can be used to design an artificial neural system for smart structures. In the paper, the characteristics and processing of piezoelectric materials are discussed, including fine-particle materials, thin film materials, active fiber composite materials, and material performance. Following this, the development of an artificial neural system using piezoceramic materials is described, then conclusions are given.

2. PIEZOELECTRIC MATERIALS

The piezoelectric effect was discovered by Pierre and Jacques Curie in 1880. It is a phenomenon in which certain crystals develop an electric charge when subjected to a mechanical strain. These materials will also expand or contract in response to an applied electric field. For piezoelectricity to exist in a material, the crystal structure of the material should be noncentrosymmetric in order to possess intrinsic polarity. There are 32 crystal classes in which all the crystalline materials belong. Twenty-one of these classes lack a center of symmetry. Twenty of the classes that lack a center of symmetry can possess piezoelectricity. Three basic steps led to the discovery and understanding of piezoelectricity in ceramics. First was the discovery of the high dielectric constant. The second step was the realization that the cause of the high dielectric constant was ferroelectricity. The third step was the discovery of the poling process in which a high voltage capable of reversing the electric moments of spontaneous polarized regions in the ceramics is applied to the material, see Cady [1].

The widespread application of the piezoelectric effect is based on ferroelectric ceramic materials. A crystal is said to be ferroelectric when it has two or more orientation states in the absence of an electrical field, and it can be shifted from one of these states to the other by an electrical field. These orientation states

are identical in the material crystal structure and differ only in the direction of the electric polarization vector at null electric field, see Lines & Glass [2, p 9]. Crystal perfection, electrical conductivity, temperature, and pressure are the factors that may affect the reversibility of polarization. Therefore, the ferroelectric character cannot be determined solely by a crystallographic structure. The highest symmetry phase compatible with the ferroelectric structure in terms of which the ferroelectric phase can be described by small perturbational structural changes is termed as the *prototype* phase. For most ferroelectrics, the prototype phase usually exists as the high temperature phase of the crystal. As a result of small structural displacements from a prototype, a typical ferroelectric possesses a spontaneous polarization P_s that decreases with increasing temperature T and disappears either continuously or discontinuously at the Curie point (T_C). For most known ferroelectrics, the onset of ferroelectricity occurs as a function of decreasing temperature.

A ferroelectric phase change represents a special class of structural phase transition characterized by the appearance of a spontaneous polarization and it exhibits dielectric hysteresis. Above the Curie point the approaching transition is generally evident by a diverging differential dielectric response or permittivity ε, which, close to T_C, varies with temperature following the Curie-Weiss law:

$$\varepsilon = \frac{C}{T - T_0} \qquad (1)$$

where T_0 is the Curie-Weiss temperature which is equal to the Curie temperature T_C only in the case of a continuous transition and C is the Curie constant. The high-temperature, prototype phase which transforms to the ferroelectric phase at T_C is called the paraelectric phase. Below T_C, in the absence of an electric field, there are at least two directions along which the spontaneous polarization can develop. To minimize the depolarizing fields, different regions of the crystal polarize in each of these directions and each volume of uniform polarization is called a *domain*. The resulting domain structure usually produces a near complete compensation of polarization. Therefore, a reversible spontaneous polarization P_S giving rise to the hysteresis loop (Figure 1) and a peak in the dielectric constant at the transition temperature T_C (Figure 2) are the signatures of a ferroelectric.

Antiferroelectrics are characterized by an antiparallel array of local dipoles with equal and opposite sublattice dipole moments that result in a net zero polarization in the crystal. Ideally, they show no dielectric hysteresis and undergo a transition to a paraelelectric phase of higher symmetry at T_C, where there is a sharp anomaly in the dielectric response. Some antiferroelectrics transform to a ferroelectric phase when heated below (T_C) or subjected to an electric field. The difference in the free energy between such antiferroelectric and the ferroelectric phases of a material is usually quite small.

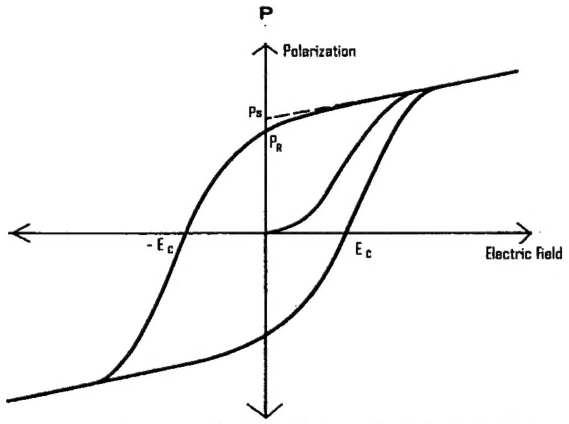

Figure 1. Hysteresis loop for a typical ferroelectric material (P_S: Saturation polarization; E_C: Coercive field; P_R:Remnant polarization)

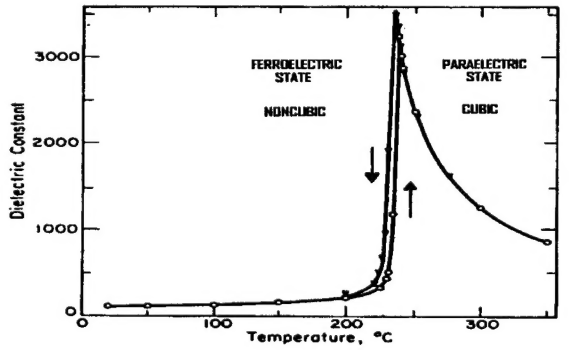

Figure 2. The anomaly in the dielectric constant versus temperature curve for $PbZrO_3$

Ferroelectrics can be classified as a *displacive* type in which the dipole moment of the unit cell vanishes in the paraelectric phase, or as an *order-disorder* type in which the dipole moment is nonvanishing but thermally averages out to zero in the paraelectric phase. In the displacive type, the displacements of the atoms in the low temperature phase are small compared to the nearest neighbor internuclear distances, whereas for the order-disorder type, the displacements are comparable to the internuclear distance. Most materials with displacive transitions have values of $C \approx 10^5$ K while those with order-disorder phase transitions have $C \approx 10^3$ K, see Burns [3, p.535]. $BaTiO_3$, $PbTiO_3$ and $KNbO_3$ are displacive type ferroelectrics; $NaNO_2$ and KNO_2 are order-disorder type ferroelectrics, whereas KH_2PO_4 is of an intermediate type.

The conceptual development of ferroelectrics is based on (a) the phenomenological thermodynamic theory of Devonshire [4-6], (b) the lattice dynamics theory of Cochran and Anderson [7-9] and (c) the microscopic statistical theory of Lines [10]. Using a thermodynamic theory, many of the changes of the macroscopic properties at the phase transitions can be interrelated, although such a theory does not give information about the microscopic nature of the transition. The phenomenological theory of Devonshire is based on the idea of an order parameter. An *order*

parameter measures the extent of the departure of the atomic (or electronic) configuration in the less symmetric phase from that in the more symmetric (prototype) phase. The appearance of an order parameter at T_C breaks the symmetry of the high temperature phase: the order parameter is zero above T_C and non-zero below T_C. In ferroelectric order-disorder transitions, the order parameter could be some measure of the amount of long range ordering of the permanent dipoles. For displacive transitions, the order parameter could be some measure of the displacement of certain ions from their high temperature equilibrium positions. For most ferroelectrics of either type, the spontaneous polarization P_S can be taken as the order parameter.

Before 1940, there were only two types of ferroelectrics: (a) Rochelle salt and some closely related tartrates, and (b) potassium dihydrogen phosphate and its isomorphs. These materials had very complicated structures and they were not very easy to synthesize. After the discovery of ferroelectricity in $BaTiO_3$ in 1941, which had a relative dielectric constant as high as 1100, piezoelectrics and ferroelectrics began to be investigated extensively. The first commercial devices made of piezoelectric $BaTiO_3$ were phonograph pickups that were marketed by Sonotone Corporation in 1947. Lead titanate was reported to be ferroelectric in 1950 on the basis of its ferroelectric to paraelectric transition at 500°C and its structural analogy with $BaTiO_3$. Antiferroelectric lead zirconate was discovered in 1951. The ferroelectric nature of ($PbZr_xTi_{1-x}O_3$) Lead Zirconate Titanate (PZT) was established in 1954 and the material became very popular because of its superior ferroelectric and piezoelectric properties. Ferroelectricity and antiferroelectricity were discovered later in various other oxides having the ABO_3 perovskite structure (Figure 3).

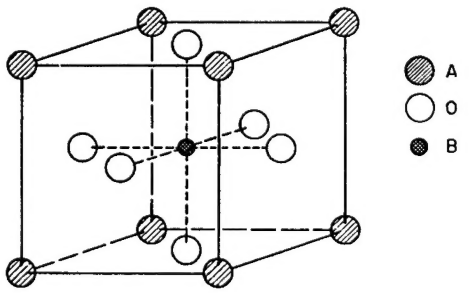

Figure 3. The perovskite unit cell.

Ferroelectricity has also been observed in stibiotantalites with the ABO_4 structure. A basic similarity between the two structures is that both consist essentially of three-dimensional networks of BO_6 octahedra with the A ions placed in interstitial positions. The ideal perovskite structure is cubic with the monovalent or divalent A ion at the cube corners, the B ions (tetra or pentavalent) at the body centers, and the O ions at the face centers (Fig. 3). The significance of the dynamic properties of the BO_6 group for the ferroelectric behavior in perovskites was first recognized by Mathias [11]. The oxygen cage remains relatively undistorted even when the overall crystal structure is considerably deformed. It is the off-centering of the B-cations (with respect to the oxygen octahedra) in the low symmetry phase that leads to the creation of a dipole moment and ultimately to the ferroelectric (FE) or antiferroelectric (AFE) ordering in such oxides. The BO_6 groups are expected to be equally important in the stibiotantalites. The temperature dependence of the soft mode in perovskites has been explained in terms of anharmonic interactions and quantitative results have been obtained using an effective quartic potential between central B and the surrounding O ions, see Bruce & Cowley [12]. It was later suggested that the behavior of the FE soft mode and related properties may be explained by the strongly anisotropic deformability of the oxygen ions, see Migoni *et al* [13]. This argument appears to be strengthened by the fact that among all the perovskites, only oxides are known to exhibit ferroelectric behavior.

Ferroelectricity and piezoelectricity have also been observed in $A_xB_2O_6$ compounds with a potassium tungsten bronze structure such as $PbNb_2O_6$, $BaNb_2O_6$ and other compounds. In bismuth layered compounds like $SrBi_2Ta_2O_9$, etc., though ferroelectricity has been observed, strong piezoelectric signals have not been obtained. Besides ferroelectrics, piezoelectricity has also been observed in other ceramics such as quartz (SiO_2), ZnO, and AlN; in organic crystals such as ammonium dihydrogen phosphate, and in polymers such as polyvinylidiene fluoride film, also called PVDF. In general, the piezoelectric materials belong to two categories; those that are ferroelectric and those that are not. Most of the piezoceramics are prepared in wafer or pellet form. The size is limited by the brittleness and cracking, and the quality of the material may decrease as size increases. In addition to wafers, there are piezoelectric composites including PZT and PLZT particle composites, see Uchino [14].

2.1 Fine-Particle Materials

In the last two decades, there has been a growing interest in the study of the properties of ultrafine particles of metals, semiconductors and oxides of various types. Corresponding to this, there has been increased activity to synthesize fine particles by various techniques. There are a large number of methods for the preparation of fine particles and nanomaterials, such as inert gas condensation, mechanical alloying, laser ablation, plasma processing, hydrothermal pyrolysis, microemulsion-based reactions, and others. By varying certain process parameters, the grain size, texture and the shape of the particles can be controlled. The method of preparation to be used depends very much on the nature of the compounds and the size range in of interest. Methods like spray-drying and liquid-drying give samples of comparatively higher size whereas purely wet chemical methods like coprecipitation, microemulsion, and sol-gel are capable of producing samples with grain size of the order of a few nanometers. The wet chemical techniques help to obtain homogeneous, single phase and stoichiometric

samples since mixing of the elements takes place at the molecular level. With such methods, it is possible to prepare fine particles of a wide variety of compounds with a controlled particle size.

The physical and electronic properties of fine particles can be much better than the properties of macroscopic materials because the fine particles can be almost defect free. The fabrication of piezoelectric materials using fine particles can increase the ruggedness and the piezoelectric coefficients of the material. The addition of small percentages of fine particles to a homogeneous material produces a composite material in which the interfacial area and grain boundaries become very large compared to the volume of the fine particles. This can greatly improve the strength, elastic modulus, and other properties of the material. Some of the methods that have been used for the preparation of ferroelectric and other fine particles are described below.

Coprecipitation. In this process, all the cations present in the solution are precipitated together by properly choosing a precipitating agent and suitably adjusting the pH of the solution. The complex that results from the coprecipitation is dried and heated at low temperature to prevent agglomeration and grain growth by diffusion across grain boundaries. The fine particles produced have a comparatively broad size distribution. This method is very useful for preparing fine particles of mixed oxides.

Sol-Gel. In this method, the cations after being coprecipitated with the help of a precipitating agent, are prevented from agglomerating while in solution by forming a concentrated suspension called the sol. This is kept in an ultrasonic bath for 15 min. to disperse the particles properly. The sol is gelated by using a dehydrating agent that removes the water from the solution, and a surfactant, which forms a layer around each particle to prevent agglomeration. The gel is dried in an oven and the dried mass is heated at different temperatures to produce the fine particles of the required size. A wide range of pure and mixed oxides can be produced by this method at temperatures much lower than required in spray-drying and liquid-drying methods. It is also possible to obtain a uniform size distribution using this method.

Microemulsions. These are thermodynamically stable, optically isotropic dispersions of aqueous and hydrocarbon liquids that are stablilized by an interfacial film of surfactant molecules. Microemulsions are generally described as monodispersed spherical droplets (50-100 Angstroms in diameter) of water in oil or oil in water depending upon the nature of the surfactants and the composition of the microemulsion. The optical transparency obtained in microemulsions is a direct function of the particle size. In order to form miroemulsions, surfactants must be selected to decrease the oil/water interfacial tension to 10^{-3} –10^{-5} mN/m. This method has been used for the preparation of fine particles of magnetic oxide, ferroelectric oxides, zinc oxide, superconducting oxides, halides, semiconductor materials, and other materials.

Rapid liquid dehydration. This process involves the selection of a water-soluble salt of the cation/cations that are present in the compound whose fine particles are to be prepared. After preparing such an aqueous salt solution, a rapid nucleation of the fine particles is initiated by pouring the aqueous solution into a dehydrating agent, which is continuously stirred by a magnetic stirrer. We have taken distilled acetone as the dehydrating agent since it has a high solubility for water but not for the salts used. The fine particles produced are collected and dried under an infrared lamp. The dried mass is then calcined at different temperatures to obtain particles of different size. Size variation can also be achieved by changing the solution concentration. This method is applicable to compounds whose cations possess water-soluble salts.

Solid State reactions. This method was used to prepare targets for laser ablation. The method involves mixing the starting compounds with the help of a mortar and pestle in acetone (to promote homogeneous mixing). The mixture is heated at high temperatures in pellet form to obtain reacted and sintered pellets for ablation. Heating was done in air as well as in a vacuum depending on the material to be prepared.

Solid-solid phase transformation. This process can be used for solids which possess a metastable polymorph. Nucleation of fine particles occurs when there is an irreversible structural transformation from the metastable phase to the thermodynamically stable polymorph. The reduction in the particle size can be related to the change in the specific volume during the transformation, and the reduction is significant for solids that undergo a relatively large change in specific volume. This method is advantageous for compounds that are difficult to prepare by wet methods due to the unavailability of soluble salts.

2.2 Thin Film Materials

For the past three or four decades, there has been considerable interest in the development of ferroelectric thin films for application in capacitors, high frequency transducers, IR vidicons, solid-state displays, and for memories. During the last few years, in particular, there has been an increase of activity in this field. This has been prompted by the emergence of new device concepts, enhanced control and analysis of film growth processes, and the availability of improved deposition and characterization facilities. There is also a need to achieve better performance in integrated circuits. Ferroelectric films with high electro-optic coefficients are well-suited for use as modulators in integrated optical circuits and as elements in large-area integrated display panels, see Francombe [15]. The development of a new generation of devices has been the major driving force behind the progress in this field. As an example, non-volatile memories with long endurance and high-speed access can overcome problems of

memory speed and volatility encountered in semiconductor and magnetic memory technologies. Researchers have also rediscovered the utility of ferroelectric materials as high-dielectric-constant capacitors. This opens up new possibilities for manufacturing planar, very high-density dynamic random access memories (DRAM). The large values of the switchable remanent polarization of ferroelectric materials are suitable for non-volatile ferroelectric random-access memories (NVFRAM), see Auciello, et al [16].

Ferroelectric films can also display a wide range of piezoelectric, pyroelectric, and electrostrictive properties, and properties for thermal insulation, hardness, reduced friction, and electrical conductivity. Piezoelectricity is being exploited in micro-machines such as accelerometers, displacement transducers and actuators such as those required for ink-jet printers, video-recorder head positioning, and micromachining. Pyroelectricity can be used in the fabrication of high-sensitivity, room temperature infrared detectors, while electro-optic activity can be used in color-filter devices, displays, image-storage systems and optical switches for integrated optical systems. Using advanced deposition methods, it has been possible to produce thin film capacitors of $Pb(Ti_{1-x}Zr_x)O_3$ (PZT) and $SrBi_2Ta_2O_9$ (SBT) with practically no polarization fatigue, long polarization retention, negligible polarization imprint, and low leakage currents, which make these suitable for integration into NVFRAMs [16]. Compared to conventional nonvolatile memories, ferroelectric memories offer the advantage of faster access times (for both reading and writing), low-voltage operation, and good read/write endurance. Moreover, in high performance multichip-module (MCM) technology, there is a vital need for the replacement of discrete passive devices that occupy a lot of space, by embedded ones. These high-density ferroelectric interconnect structures will play a significant role in nondigital electronic modules including mixed-mode circuits, power conversion, and optoelectronics, see Dey, et al [17]. Ferroelectric thin films are also used in microelectromechanical systems (MEMS) which combine traditional Si integrated circuits with micromechanical sensing and actuating components. A goal of MEMS is to develop a smart structure with a self-contained system of interrelated sensing and actuating devices together with signal processing and control electronics on a common substrate. MEMS are already being used in flowmeters, pumps, motors, and other devices, see Polla, et al [18]. Various techniques have been used for the deposition of epitaxial and polycrystalline thin films. Some of the more important techniques are described briefly.

Evaporation. This is one of the oldest techniques used for thin film deposition and involves removal of atoms from the source by thermal means, see Ohring [19, p. 82]. High deposition rates, clean environments for film formation and growth, and general applicability to many classes of materials have made this technique very popular. It has also been used for the preparation of mixed oxides such as $BaTiO_3$, see Yano, et al [20].

Sputtering. In this method, atoms are dislodged from the surface of a solid target through the impact of gaseous ions. This method can be used for compounds with stringent stoichiometry limits. The adhesion of the film to the substrate is very good. The target is a plate of the material to be deposited, which is connected to the negative terminal of a DC or RF power supply. The substrate, which faces the target, is grounded or biased positively and is heated to a specified temperature. After evacuation of the chamber, generally Ar gas is introduced. Positive ions in the discharge strike the cathode plate and eject neutral target atoms which get deposited on the substrate [19, p. 121]. DC sputtering is used for metals and alloys whereas RF sputtering is used for insulating as well as conducting materials. In magnetron sputtering, a magnetic field is superimposed on the electric field between the substrate and the target to produce larger discharge currents, which increases sputter deposition rates. Sputtering has been used for the deposition of films of single elements like Al, Cr, Ge, and W; for alloys like Al-Cu, Gd-Co, and Co-Ni-Cr; for borides like TiB_2 and ZrB_2; for carbides like SiC, TaC, and WC; and for oxides like Al_2O_3, CeO_2, SiO_2, $BaTiO_3$, $PbTiO_3$, PZT, MgO, YFe_2O_3; and many other compounds.

Molecular beam epitaxy (MBE). This is the epitaxial growth of a substance on a substrate resulting from the condensation of directed beams of molecules or atoms in a high vacuum, see Chang, et al [21]. The beams are created from sources contained in effusion ovens where thermal equilibrium is maintained. The deposition process at the substrate is governed by the kinetics. This technique requires ultra high vacuum and a spectrometric analyzer to monitor the flux of the component vapor species and the environment in which the film is grown. The method is characterized by a slow growth rate and low growth temperature. Since the constituent components are impinged upon the substrate from different beams, both the composition and the dopant concentration can be controlled conveniently. These properties facilitate the use of this technique in growing structures where abrupt changes of the composition and doping are required. The slow growth rate makes precise thickness control possible and the low temperature minimizes undesirable thermally activated processes such as diffusion. Superlattices, which are structures composed of thin, periodically alternating single-crystalline layers, can be grown very accurately.

Chemical vapor deposition (CVD). This process involves reacting a volatile compound of the material to be deposited with volatile phases of other compounds to form a nonvolatile solid that deposits atomistically on a suitably placed substrate, see Kern & Ban, et al [22]. Films produced by CVD have found applications in diverse technologies such as fabrication of solid-state electronic devices, manufacture of ball-bearings and cutting tools, and the production of rocket engine and

nuclear reactor components. The importance of CVD is growing rapidly because it can produce, at relatively low temperatures, thin films of a large variety of elements and compounds in either crystalline or amorphous form with a high degree of perfection and purity. Further advantages of CVD include the relative ease of creating materials with a wide range of accurately controllable composition and layer structures that are difficult or impossible to attain by other methods. An additional advantage is that CVD is a low-cost technique. With the help of CVD, it is possible to produce films of oxides SiO_2, Al_2O_3, and Nb_2O_5, silicates, nitrides and oxynitrides; group IV, III-V, II-VI and other types of semiconductors; metals and alloys; and superconductors and ferroelectrics. Low-pressure CVD (LPCVD) involves low-pressure reactor systems for use in the semiconductor industry especially for depositing polysilicon films. In plasma-enhanced CVD (PECVD), glow discharge plasmas are sustained within chambers where simultaneous CVD reactions can occur and hence causes chemical reactions to occur at a comparatively lower temperature. Laser enhanced CVD (LECVD) involves the use of monochromatic photons to enhance and control the reactions at the substrate.

Solution technique. Films may be deposited on substrates by chemical or electrochemical means from solutions. Ferrites, high-T_C superconductors, dielectrics, and antireflection coatings are among the electroceramics on which solution deposition has had a significant impact. It also facilitates better stoichiometic control of complex oxides than rf-sputtering and MOCVD, and it can cover wide ranges of film composition. Most solution approaches may be grouped into three categories: (i) sol-gel processes that use 2-methoxyethanol as reactant and solvent, (ii) hybrid processes that use chelating agents such as acetic acid to reduce alkoxide reactivity, and (iii) metalorganic decomposition (MOD) approaches that use water-insensitive carboxylate compounds, see Tuttle et al [23]. The sol-gel method based on controlled hydrolysis of metal alkoxides has been used extensively for the preparation of thin films of ABO_3 type compounds. Another useful solution technique is spray-pyrolysis, which involves spraying a solution, usually aqueous, containing soluble salts of the atoms of the desired compound on to a heated substrate where the droplets undergo pyrolytic decomposition and form a single crystallite or a cluster of crystallites of the product. This method has been used for various oxides, sulphides, and selenides, see Chopra et al [24].

Pulsed laser ablation deposition (PLAD). In this technique, a pulsed laser beam (usually an excimer laser) is directed on a solid target. The interaction of the laser beam with the target produces a plume of material that is transported towards a heated substrate placed directly in the line of the plume. The two most important features of PLAD are its ability to precisely control the composition of compounds containing as many as six elements and the ability to operate in high partial pressures of reactive gases which helps in maintaining the correct abundance of volatile elements. With no ion or evaporation sources that contain hot filaments in the vacuum, PLAD is possible at ~100-400 mTorr pressure of reactive gases like oxygen. Since PLAD can transfer the composition of the target to the deposited film, it has been successful in the fabrication of complex oxides whose constituents can have vapor pressures that differ by 10^6. It has been extensively used for preparing films of high-T_C oxides, ferroelectrics, ferrites, semiconductors, metals and alloys. Films of diamond-like carbon, polymers, and biocompatible films and superlattices of various compounds have been deposited by this technique.

Alhough it is a very popular technique for the deposition of thin films, PLAD has a few disadvantages: (i) uniform coating of large areas substrates has not been achieved for most materials because of the narrow forward angular distribution, and (ii) films show the presence of micron sized particulates though the particulate density and size distribution has been controlled, see Auciello et al [25, 26], and Hubler [27].

Electrostatic-Self-Assembly (EAS). Electrostatic-Self-Assembly (EAS) also referred to as Ionic Self-Assembled Monolayers (ISAM), and can be used to fabricate very thin polymer films by the alternate absorption of anionic and cationic polymers. The thin monolayer films can have special performance characteristics including piezoelectric properties. The piezoelectric polymer films can be produced at room temperature and the film does not require poling. Increasing the strain coefficients and the thickness of the films is necessary for them to be used in more widespread applications.

2.3 Piezoceramic Fiber Composites

Piezoceramic fiber materials are constructed from thin PZT fibers that are embedded in an epoxy matrix. Electrodes are placed on the epoxy above the fibers in an interdigital or other pattern that is symmetric on the top and bottom. The electrodes are covered with capton sheets, and the fibers are poled longitudinally. These Active Fiber Composites (AFC) [28-30] or Macro-Fiber Composites (MFC) [31] have the advantage of being flexible, conformable, and more rugged than monolithic PZT. If a fiber breaks, the fiber can still actuate or sense, and the crack does not propagate as in a monolithic PZT. The AFC also is a unidirectional actuator or sensor. A preform before electroding and poling that is used to build an AFC is shown in Fig. 4.

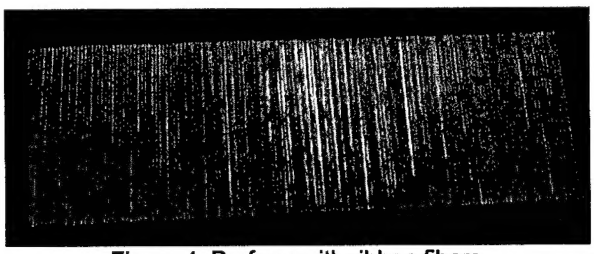

Figure 4. Preform with ribbon fibers.

The material process to produce AFC fibers uses extrusion [30] to produce green piezoceramic fibers that are then fired. Fibers up to 0.2 m in length and with thickness of 100-250 microns can be produced. The MFC fibers are produced by slicing a monolithic wafer and assembling them similarly as with the AFC. The AFC/MFC have a higher actuation performance in the plane than monolithic PZT, but the poling and actuation voltage is higher than for poling monolithic PZT through the thickness.

2.4 Piezoelectric Material Performance

The most common piezoelectric ceramic used for sensors and actuators may be PZT because of its large piezoelectric strain coefficient. Since the PZT material is crystalline, it consists of unit cells. A unit cell is the smallest 3-D repeating atomic unit whose shape allows crystal symmetry in PZT. A dipole results from a difference between the center of the positive charges and the center of the negative charges in the unit cell. The most common PZT materials produced thus far are monolithic polycrystaline piezoceramics, which have a random agglomeration of small crystals. Poling switches the polar axes of the small crystals in the polycrystaline ceramic to those directions allowed by symmetry which are nearest to aligning with the applied electric field. A single-crystal consists of identical unit cells that have their dipole axes aligned in the same direction. Single crystal piezoceramics have piezoelectric coefficients that are about a factor of five greater than the coefficients of polycrystaline PZT. However, single crystal piezoceramics are presently difficult to produce.

There are a number of limitations of piezoceramic materials that have restricted their use as sensors and actuators depending on the structural application. These are that the induced stresses and strains are small, the piezoceramics are brittle, the material can depole at high compressive stress and at high temperatures, the cost is high, PZT is a toxic material that is not bio-degradable, the material ages, hysteresis and heating occur at high frequencies, the PZT cannot sense static loads, compliance in the bonding layer can reduce the transduction efficiency, the wiring and embedding can cause cracking in structures, and the piezoceramic materials are heavy. For AFC's, they require a high voltage to pole, PZT fibers are expensive to make, and the electroding may affect wave propagation. Also, the charge produced by the PZT becomes a factor in sensor design. For an open circuit, the voltage generated by a PZT wafer is independent of the area of the sensor element. However, when building self-powered continuous sensor circuits with many nodes, there is series resistance in the circuit and impedance of the measuring instrument. The voltage output thus depends on the charge produced, which depends on the size of the sensor element. If thin film sensor elements are used, the charge produced is small. In this case, a charge amplifier might be needed for each sensor node, or group of sensor nodes.

Some of the important parameters that describe the transduction properties of piezoelectric materials are discussed here. The piezoelectric strain coefficient d_{ij} is used to characterize the actuation capability of piezoelectric materials. It relates the strain in the material to the applied electric field, and is:

$$d_{ij} = S_{jj} / E_i^T \qquad (2)$$

where i is the direction of the electric field, j is the direction of the resulting normal strain, S_{jj} is the strain in the piezoelectric material, and E_i^T is the voltage field in the material at a constant stress level, which is usually the free strain unclamped condition. The piezoelectric voltage coefficient relates the voltage output to the stress in the material and is:

$$g_{ij} = E_i / T_{jj}^D \qquad (3)$$

where T_{jj}^D is the stress in the material when the electrical displacement D is constant, which is usually the open circuit condition. The g_{ij} coefficient is used to characterize the sensing capability of piezoelectric materials. It should be noted that the impedance of the sensor material must be matched to the impedance of the structure to obtain the maximum power transfer between the structure and the PZT. For sensing and actuation applications when the structure is stiff such as an aluminum or graphite-epoxy aircraft component, a material such as PZT-5A with a large d_{ij} coefficient is usually desired. In the case of a flexible structure such as an inflatable structure or tire, a material such as PVDF with a large g_{ij} coefficient is usually desired.

The electromechanical coupling coefficient for a single direction is:

$$k^2 = \frac{ME_{out}}{EE_{input}} = \frac{EE_{out}}{ME_{input}} \qquad (4)$$

where *ME* and *EE* are the mechanical and electrical energy input and output. The direct and planar coupling coefficients k^2 are about 0.5 and 0.4, while the transverse coupling coefficient is about 0.1.

The capacitance is an important in designing sensors/actuators using piezoceramic materials and is given by:

$$C = K\varepsilon_o A / t \qquad (5)$$

where K, ε_o, A, t represent the relative dielectric constant, the dielectric constant for air, the surface area on one side or face of the piezoceramic that is electroded, and the spacing between the electrodes, respectively. Minimizing the capacitance is desired to increase the voltage output in sensor circuits, and to reduce the power required from an amplifier to drive PZT actuators at high frequency.

The dielectric loss factor, $\tan\delta_c$, is a measure the electrical hystersis loss in the material. Minimizing the dielectric loss of PZT is important for certain applications [32]. For sensing applications where the voltage output level and signal-to-noise ratio are important, non-ferroelectric Aluminum Nitride (AlN) is a competitive material. Having reviewed the

characteristics and performance of piezoelectric materials, also see Jaffe [33], the design of a sensor system for smart structures is discussed next.

3. AN ARTIFICIAL NEURAL SYSTEM

A simple and low cost method is needed to assess the physical condition of large components and structures including aging and new aircraft, spacecraft, bridges, buildings, rockets, pressure vessels, pipelines, and also spatially periodic structures such as bearings and turbine components. The concept of a Structural Condition Monitoring (SCM) system that is integrated within the structural material potentially can revolutionize the manner in which structural systems are maintained by providing a real-time assessment of the performance capabilities and safety of structures. This will eliminate the need for scheduled inspections and periodic replacement of parts and allow the most efficient use of structures while avoiding catastrophic failures. It will also lead to new aerospace and transportation systems that are more reliable, durable, efficient, safe, and less expensive to operate and maintain.

Present techniques for in-situ real-time SCM lack sensitivity for use on structures that have complex geometry such as joints, ribs, varying thickness, fasteners, and varying curvature. Also, the cost and complexity of these systems for use on large structures would be high. The most promising of the present techniques use Lamb wave propagation in the plane of the material to detect damage. These methods can detect damage accurately in simple structures by wave reflections from defects, see Wang, et al [34], or by transmitting and receiving waves and casting shadows, see Schwarz, et al [35]. However, for some applications these approaches may be too complex because large arrays of sensor/actuator elements will be required. The associated wiring, instrumentation, amplification, multiplexing, and computational resources required to implement these methods on a large scale may be prohibitive in terms of cost, added weight, and reliability. Another difficulty with these methods is that individual monolithic piezoceramic wafers are used as the sensor/actuator elements. These elements and their connections form stress concentrations in composite materials that might lead to cracking and failure of the structure. Another possible approach for SCM is to monitor Acoustic Emissions (AE) caused by damage growth. AE methods have been used in critical areas of aircraft and other structures in a few exploratory studies and have been effective in detecting small cracks in the neighborhood of the sensor. However, application of the conventional AE technique to SCM has been limited in practice. This is because it is impractical to embed or incorporate on the structure a large number of conventional AE sensors and signal processing channels, and because the AE waveforms that travel any significant distance are too complicated for purposes of source characterization. A third approach for SCM is to monitor dynamic strains over the structure. This approach is at present difficult to implement because strain transducers such as optical fibers with Bragg gratings provide a very localized measurement only at each grating. This means that a very large number of fibers and gratings would be required to monitor large or complex structures to detect small damage. The manufacturing of the structure with the optical connections, and the multiplexer and optical analyzer would become complex and expensive. After reviewing existing techniques, it is evident that in spite of the need and potential for large cost savings and increased safety and reliabililty, there has not been any general technique put into use for SCM.

Recently, a new continuous sensor design has been proposed using serially connected piezoceramic sensor elements, see Sundaresan et al [36]. It has been demonstrated that this sensor arrangement can improve dynamic strain and AE monitoring by reducing the number of signal processing channels as well as sensor elements by a factor of up to sixteen. This sensor concept is being extended to mimic the nerve cell and the human nervous system, see Sundaresan et al [37]. Initial research is being performed to investigate the rules and principles that govern the function, structure (physical constraints on function), and operation of the biological nervous system (neuroscience), and to mimic these functions to develop an Artificial Neural System (ANS). The ANS is in the initial stages of being built using engineering materials and microelectronics. Here, we will briefly discuss sensory signal processing in the biological neural system. We will then apply these principles to illustrate how to build an artificial nerves using PZT materials. Biological and concept structural nerve cells are shown in Fig. 5.

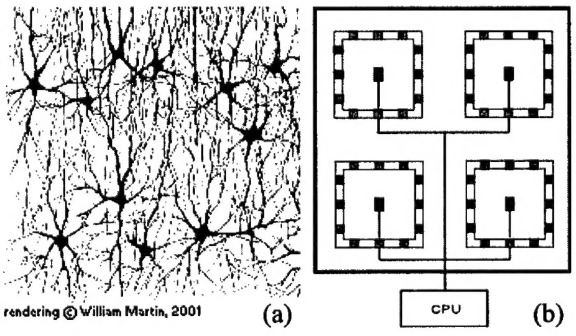

Figure 5. Biological (a) and structural (b) nerves.

We discuss neuronal morphology and the replication of cellular functions using smart materials and microelectronics. The neuron is the fundamental processing unit in the nervous system, see Zigmond et al [38]. It consists of three functional segments: several to hundreds of thin processes called *dendrites*, which act as inputs; the *soma*, or cell body, that acts as the processor; and a long thin process called the *axon*, which acts as the output. The neuron integrates several amplitude-modulated analog inputs to produce a frequency-modulated digital output. The function of the

neuron can be understood in terms of the two component model shown in Fig. 6, which treats neuronal processes as leaky electrical cables. The highly nonlinear voltage dependent membrane properties produce all-or-none responses called *action potentials* in the axon. There are many millions of neurons and interneuronal connections in biological systems. By understanding the structure and function of the neuron, we can mimic its pertinent functions for application to SCM. Considering the different forms of piezoceramics discussed, it is most practical to build the cell dendrites using the piezoceramic ribbon fibers shown in Fig. 4. These ribbons conceptually will be poled using a transverse method, not in-plane as other AFC materials. The soma will be replicated using an Application Specific Integrated Circuit (ASIC), and the axon is replicated using a digital data bus. The piezoceramic ribbon dendrites will be discussed in this paper. Other aspects of the ANS are given in Ghoshal, Martin, Schulz, Sundaresan et al [39-43]. A concept ribbon with series electroding is shown in Figure 7. The sensor segments in the ribbons are called nodes (orange and green). The maximum length and number of dendrites per unit nerve cell depends on the capacitance and resistance of the piezoceramic fibers. The nodes will be poled by placing temporary electrodes over the top and bottom surfaces of the preform. After poling and removal of the temporary electrodes, this will produce a series connection of the nodes which reduces the capacitance of the sensor and increases the voltage. The dendrites will be constructed of five or more parallel ribbons and the continuous sensor will be self-powered, small, conformable, rugged, and will be sensitive along its entire length.

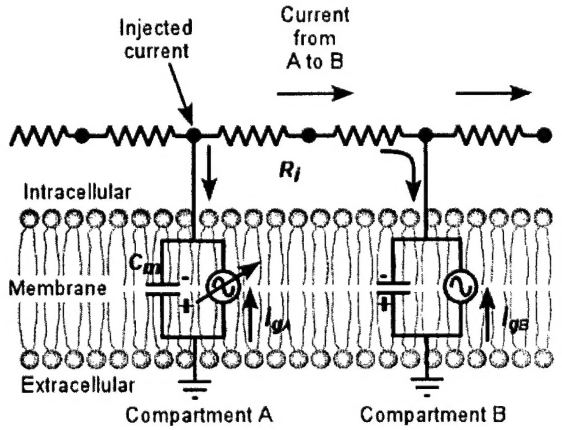

Figure 6. Equivalent circuit of two neighboring segments A, B of a dendrite or axon showing pathways for current spread in response to an input at A.

The ASIC and the digital data bus are available commercially for a pressure sensing application and can be re-designed for use with the neural system, see [44]. The piezoelectric constitutive equations and an electrical circuit model have been developed to model the basic ANS. The basic linear passive functions of the neuron are understood and can be replicated using piezoceramic ribbon fibers, and by using existing ASIC technology. However, the nonlinear and active properties of the neural system need to be modeled and replicated using microelectronics. The nonlinear and active properties of neurons [38] are important to include in the neural architecture to achieve a spatially dense coverage of the dendrites using a small number of Transducer Bus Interface Modules (TBIM) which contain the ASIC chips. Simultaneous sensing at many dendrites will produce an additive signal response that will provide a stronger signal to indicate damage. This will reduce the cost and complexity of the ANS.

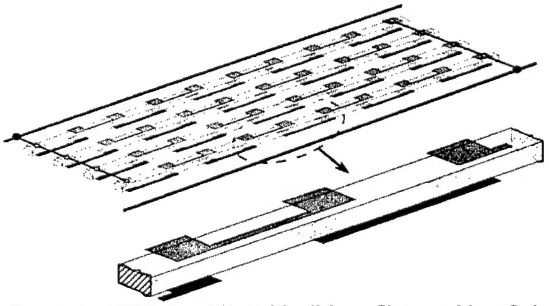

Figure 7. PZT dendrite with ribbon fibers with a 3:1 aspect ratio ($600\times200\mu-m$).

Major benefits from the piezoceramic fiber sensor system are summarized as: (a) unidirectional sensitivity, (b) self-powered, (c) conformable, (d) the sensor will have high energy coupling because the electric field is not reduced as a result of the matrix dielectric material, (e) the d_{31} sensing is practical to use because the electroding can be put directly on the fiber, and (f) the interdigitated electrode layers above and below the fibers in active fiber composites are eliminated in the new design, this eliminates the small wave reflections that occur from each electrode which can add up to cause a significant decrease in the energy of high frequency waves.

3.1 Modeling a Neural Sensor

We have developed an algorithm to study the benefits of the ANS. The algorithm computes the response of the nerve fibers as a result of acoustic waves propagating in a plate. The algorithm uses the parameters of the nerves, the one-dimensional piezoelectric constitutive equation, and a specified acoustic waveform, and it computes the voltage as the wave passes over the sensor nodes. Because of the piezoelectric properties of the nerve fiber, its nodes can be modeled as a capacitor in parallel with a current source. The piezoelectric constitutive equations are listed in the IEEE standard ANSI/IEEE Std. 176-1987. This standard is used to derive the basis of the AFC electrical modeling. Equations from the IEEE standard on piezoelectrics can be put into matrix form to give the piezoelectric constitutive equations:

$$\begin{bmatrix} D \\ T \end{bmatrix} = \begin{bmatrix} \varepsilon^S & e \\ -e_t & c^E \end{bmatrix} \cdot \begin{bmatrix} E \\ S \end{bmatrix}, \begin{bmatrix} D \\ S \end{bmatrix} = \begin{bmatrix} \varepsilon^T & d \\ d_t & s^E \end{bmatrix} \cdot \begin{bmatrix} E \\ T \end{bmatrix} \quad (6, 7)$$

In these relations, the induced strain constants form a 3 by 6 matrix with components d_{ij} (m/V) given in equation (2), ε^S is a 3 by 3 matrix describing the permittivity components ε_{ij} (farads/m) under a constant strain condition given in equation (3), and the superscript T indicates a constant stress condition. The induced stress is a 3 by 3 matrix of the components e_{ij} (Coulomb/m^2). The subscript t means transposed. The compliance matrix is a 6 by 6 matrix with components s^E_{ij} (m^2/N). The stiffness matrix is a 6 by 6 matrix with components c^E_{ij} (N/m^2). D_i is the electrical displacement (Coulombs/m^2), T_i is the stress (N/m^2), E_i is the electric field (V/m), and S_i is the strain (m/m). If the electric field is only applied through one axis, and we neglect any actuation transverse to the fiber direction, then scalar values can be used in equations (6) and (7), assuming that the ribbon fibers exhibit linear bulk piezoceramic properties. Algebraic comparison of the two forms of the piezoelectric constitutive equations shows that:

$$e = dc^E, \tag{8}$$

which can be readily calculated from the material properties. From equation (6), the electrical displacement is:

$$D = \varepsilon^S E + eS. \tag{9}$$

Let C be the capacitance of the nerve sensor, with an effective capacitor area of A_e, and effective plate separation distance h. Then the capacitance can be expressed as:

$$C = \varepsilon \frac{A_e}{h}. \tag{10}$$

By letting $\varepsilon=\varepsilon^S$, then $\varepsilon^S=(Ch/A_e)$, equation (9) becomes:

$$D = \frac{Ch}{A_e} E + eS \tag{11}$$

Multiplying equation (11) by A_e, and substituting E=V/h gives:

$$Q = CV + eA_eS \tag{12}$$

The time derivative of equation (12) gives the current *i* going through the nerve sensor. The calculation of the current *i* in the circuit is:

$$i = C\dot{V} + eA_e\dot{S}. \tag{13}$$

Equation (13) can be represented by the electrical circuit shown in Figure 8, where i_c represents the component of the current going through the capacitor of the model, and i_g represents the component of the current generated by the piezoelectric fibers. The sensor nodes form a series connected continuous sensor as was shown in Figure 7. With this arrangement, and using the results from the constitutive equations, an analytical expression for the circuit voltage can be computed. This voltage is proportional to the dynamic strain in the structure at the sensor and thus can be used to detect damage through direct strain measurements or wave propagation parameters and acoustic emissions. From Figure 8 and using Kirchoff's Voltage Law, we can see that for n sensor nodes we obtain the current equation:

$$\frac{d}{dt}(i) + \frac{n \cdot i}{RC} = \frac{eA_e}{RC} \sum_{j=1}^{n} \dot{S}_j \tag{14}$$

The homogeneous and particular solutions for Equation (14) must be calculated and added for the total solution of the current *i*. The product of the current i(*t*), and the impedance *R* of the measuring device equals the voltage of the series connected sensors as a function of time. Thus, we solve for the current to get the voltage:

$$V_0 = iR \tag{15}$$

Because the term on the right hand side of Equation (14) depends on the strains imposed upon each sensor node in the series, it is difficult to get a closed form solution for the current. Thus, a Newmark-Beta explicit integration method with a force balance iteration is used to solve for the current. To simplify the computations when modeling one-dimensional wave propagation, a voltage divider is assumed and the voltage is reduced by one-half. This approximation is reasonable and has been verified on other problems.

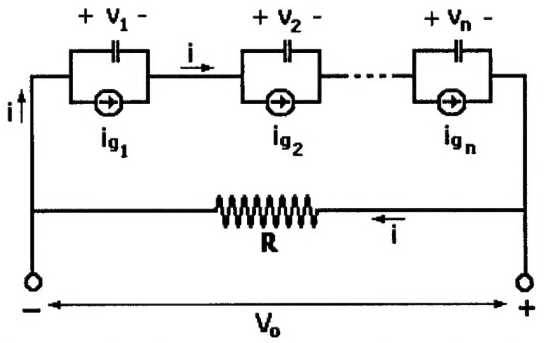

Figure 8. Circuit model of the nerve fiber with nodes 1,2,...n connected in series.

The key result of this analysis is contained in Equation (14). To obtain the maximum sensitivity from the continuous sensor we must make the right hand side of Equation (14) as large as possible. Because the strain levels in the structure are produced by acoustic emissions from damage, the sensor should be as close as possible to the damage. This is an advantage of using the ANS, it can be distributed over the full structure. The sensor parameters in this equation must also optimized. The resistance value in the circuit is the combination of the resistance of the ANS electroding and the impedance of the measuring instrument. For the series connectivity of the sensor nodes, the capacitance adds as the sums of reciprocals and therefore reduces the overall capacitance, but the resistors in series add directly. This analysis illustrates the advantage of the series sensor design and that the resistance of the AFC nodes must be small.

This model of the ANS nerve fiber is similar to the electrical model of the nerve cell in Figure 6. Note that the nerve cell has the capacitors in parallel with a current source and the nerve cell can sense along its length. The artificial nerve is similar in behavior and modeling to the nerve cell, but the stimulus is by electro-chemical processes in the biological cell and by peizoelectric processes in the structural material. Figure 9 is an illustration of an ANS that we have designed to amplify and filter the structural response. The nerve is actually a spatial filter that uses the alternating polarity and the series connectivity of the sensor nodes to

multiply the amplitude of the signal, compared to a conventional single point sensor. The filter also cuts-off low frequency waves that are not of interest for damage detection. Waves that have a much shorter wavelength than λ (higher frequency waves) will not be amplified, waves that have a wavelength of λ will be amplified, and waves that have a much longer wavelength than λ (lower frequency waves) will be attenuated. The pitch (p) of the sensor nodes in Figure 9 is constant, but a variable pitch sensor can also be designed to widen the bandwidth of the sensor. The nerve fiber with variable pitch is a very exciting concept that can improve the accuracy and practicality of damage detection. There can be two or more pass bands of the filter to allow measurement of low frequency dynamic strains for performance and loads monitoring, and a high frequency pass band to monitor the structure for acoustic waves caused by damage. The concept of using active fiber composite materials as sensors is an exciting new field with many opportunities for improving sensing and consequently the reliability and later the vibration control of structures.

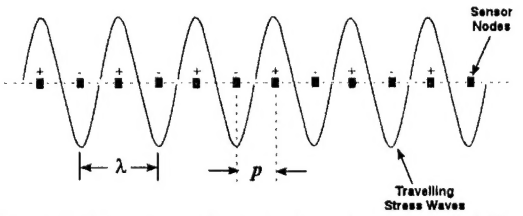

Figure 9. The nerve fiber designed as a spatial filter where the nodes have a constant pitch, series connectivity, and alternating polarity.

3.2 1-D Wave Propagation Simulation

A 1-D wave propagation analysis is presented here to show the advantage of the ANS. The objective of the analysis is to determine the optimal sensor configuration to detect acoustic waves in the structure that are a result of damage. The electrical circuit model of the nerve fiber is used and different waves are propagated along the sensor. The parameters used in the sensor analysis are given as follows. The time step is 0.1 micro-second; the acoustic wave frequency was varied from 1 KHz to 2 MHz; the modulus of elasticity of the fiberglass composite plate is 25 GPa; the mass density of the plate is 1799 kg/m^3; the velocity of propagation of waves in the plate is 3,714 m/sec; the width of the ribbon fiber is 265 microns; the length of the ribbon fiber is 20.6 cm; the width of the fiber is 0.795 mm; the electroded length of each sensor node is 6.3 mm; there are 12 nodes on the fiber; there are 12 fibers parallel in one layer that are used to form the sensor; the modulus of elasticity of the PZT 5A material is 5.6 GPa; the induced strain constant $d_{13} = 155 \times 10^{-12}$ m/volt; the electrode area of one node is 4.97 micro-m squared; the capacitance of one sensor node is 0.058 nano-farads; and the induced stress constant of the PZT material is e=8.68 N/(Volt*m) or coulomb/m^2. The amplitude of the excitation strain wave is 1 micro-strain. This is the approximate level of strain in AE waves caused by cracks. The damping ratio for all frequencies for the fiberglass material is 0.03. The damping causes the wave amplitudes to decay in time with the higher frequency waves decaying in a shorter time and distance than the low frequency waves. The wavelength of the modes is computed as:

$$\lambda = v / f \qquad (15)$$

where v is the wave velocity and f is the frequency of the wave. As an example, for the 0.25 MHz wave $\lambda = 3714/0.25 \times 10^6 = 14.84mm(0.584inches)$. The pitch of the sensor nodes is then given as:

$$p = \lambda / 2 \qquad (16)$$

Therefore, for this example the pitch of the sensor nodes is, $p = 7.42mm(0.292inches)$. This pitch will work for the same or alternating polarity configurations of electroding. In addition, the electrode spacing can be chosen to amplify the acoustic signal, which is not possible using a single sensor. This shows that thin electrodes and small pitch are needed to capture the high frequency waves. The sensor ribbon nodes are modeled as poled effectively in series to yield higher sensitivity to in-plane and bending strain and to transverse impact. The sensor would be constructed by individually electroding each ribbon. Segmented electrode sections can be deposited directly on each ribbon for the highest sensitivity possible. This will produce high energy coupling because the electric field is not reduced as a result of the matrix dielectric material.

The new ANS will be flexible, fracture tolerant, unidirectional, and the d_{31} sensing may be more practical to use because the electroding can be put directly on the fiber, and the poling is simple and at low voltage, about 200 volts using a technique briefly described in the statement of work section. Furthermore, the sensor density can be increased to improve sensitivity whereas the using the interdigital electroding to achieve the higher d_{33} coefficient may introduce stress concentrations in the fiber due to non-uniformity of the electric field, increase the possibility of dielectric breakdown when small cracks develop in the composite matrix material, which is common in composite materials, and there would be wave interaction and attenuation by the upper and lower electrode layers. For high-frequency sensing applications, there are significant advantages of the design proposed, including series connectivity, alternating poling directions, and direct electroding. The new sensor design is aimed to overcome the limitations and improve the sensitivity, ease of manufacture, and prevent wave distortions for sensing high-frequency waves.

When designing a sensor, the stress-state in the structural material and the ANS must also be considered. In composite materials, the fibers should be monitored using a parallel unidirectional sensor. The ANS will be mainly sensitive to axial stress in the fiber. Thus, the ANS can be integrated into a composite with

the fiber direction parallel to the structural fiber direction. The ANS can be designed just as an anisotropic composite material with the sensor close to any high stress sites. The ANS will carry some structural load, and it is thin and parallel to the structural fibers and will not significantly affect the strength of the composite.

The results of a one-dimensional wave propagation analysis are discussed next. The acoustic waveform used for testing is shown in Figure 10. The frequency of the waveform shown is 250 KHz and it is varied in the analysis. It is crucial to detect the high-frequency leading part of acoustic waves to identify damage. The later parts of the waveform change as the wave travels away from the source because of dispersion in wave propagation and due to combination with other signals. Therefore, it is most important to be near the damage and to detect the high-frequency leading part of the waveform. The ANS is highly distributed and therefore will be close to the damage locations. Here we have designed the ANS to detect waves with frequencies around 250 KHz, which is a frequency where AE's typically occur in composite materials.

Figure 11 shows the ANS response caused by an acoustic wave with a frequency of 1 MHz. Figure 12 shows the AFS response caused by an acoustic wave with a frequency of 250 KHz. Figure 13 shows the ANS response caused by an acoustic wave with a frequency of 1 KHz. The voltage level of 0.2 to 0.32 volts is sufficiently high to give a good signal to noise ratio, and the waveforms are very clear reproducing the AE wave at frequencies at or above 250 KHz. The 1 KHz wave is mostly attenuated as desired. These plots show that as the frequency of the acoustic wave decreases below the design frequency, the voltage output of the sensor also decreases. This is because the pitch of the sensor nodes is smaller than the wavelength of the acoustic wave, and because the nodes of the ANS are connected with alternating polarities. This sensor design thus will spatially filter and cancel waves that have longer wavelengths and lower frequencies than for which the sensor was designed. This design is similar to a Surface Acoustic Wave (SAW) device except that we are using the sensor inside the structural material but near the surface, and our design works at lower frequencies than typical SAW devices used in cell phones and other communication applications. The design analyzed can detect AE signals with frequencies above 250 KHz and it cancels low frequency waves that are due to normal structural responses.

This simulation study shows two advantages of the new electoding pattern: first it can be adjusted to match the wavelength of the modes of the desired frequencies to amplify the signal voltage, and second it can spatially filter out the lower frequency responses from the signal that are due to normal structural vibrations.

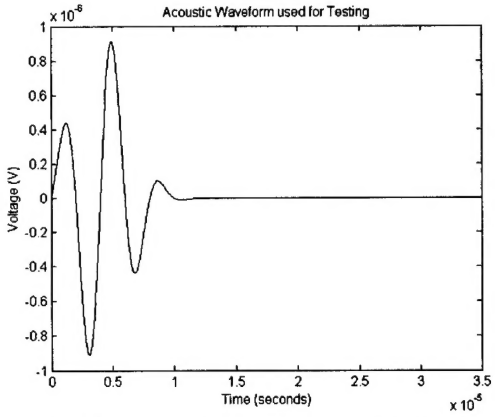

Figure 10. The acoustic waveform used for testing the AFS (a 250 KHz wave is shown).

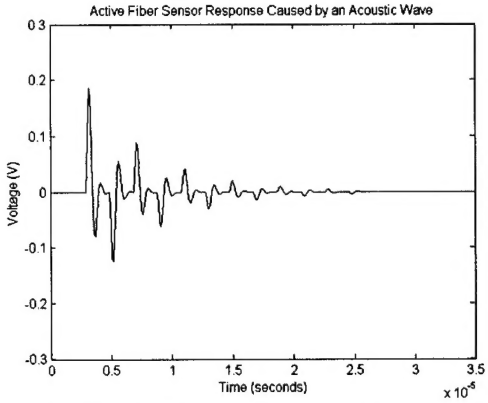

Figure 11. The AFS response caused by an acoustic wave with a frequency of 1 MHz.

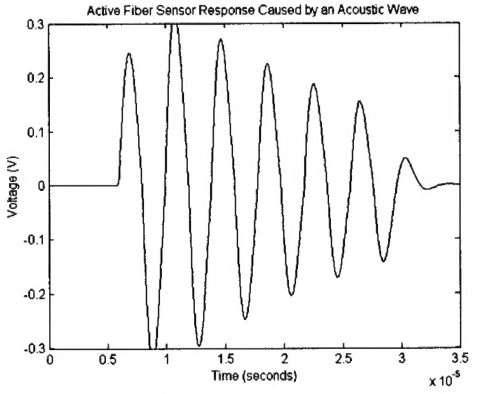

Figure 12. The AFS response caused by an acoustic wave with a frequency of 250 KHz.

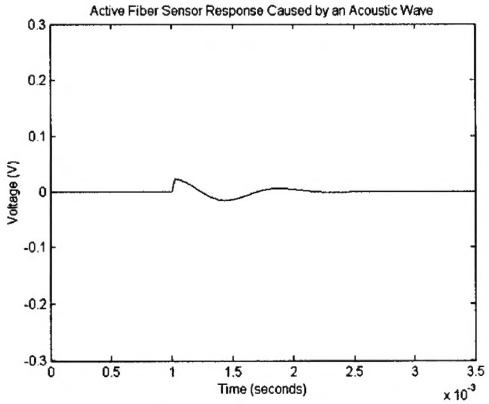

Figure 13. The AFS response caused by an acoustic wave with a frequency of 1 KHz.

3.3 Experimentation

Experiments are being performed to verify the characteristics and potential of the ANS. Standard discrete 1.27cm * 0.95cm * 0.25mm PZT sensors are used in this experiment in order to present the concept. The small size of the PZT's will allow higher frequency components of acoustic waves to be measured. The PZT patches sense strain in any direction in the plane of the plate. All of the PZT sensors are connected serially to form one continuous sensor with only one channel of data acquisition to a digital oscilloscope. Pencil lead breaks using a 0.3mm lead are used to simulate AE. The data is collected through a single channel to a digital oscilloscope and then downloaded on a laptop for plotting. The experiment is performed using a 0.91m * 1.2m * 6.3mm fiberglass panel (Fig. 14) with the continuous sensor.

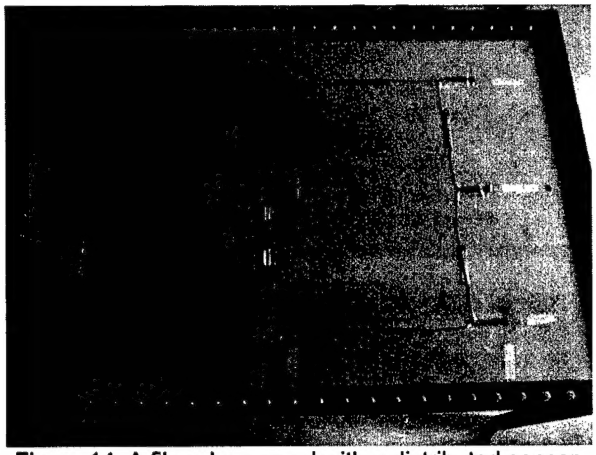

Figure 14. A fiberglass panel with a distributed sensor.

The voltage response due to a lead break on the panel is shown in Figure 15. The experiment with the composite panel showed that the energy levels from AE captured by the continuous sensor are considerably higher than for a single sensor that is far away from the lead break. This is because damping causes much higher attenuation in composites and high frequency data is lost when the AE source is away from the sensor. The amplitude of the simulation results was decreased by a factor of 7.5 to compare to the experimental results. The lower amplitude in the test is thought to be due to shear lag in the bonding and capton film that attach the PZT to the panel. The short length of the PZT element may not allow full shear transfer, and this is being investigated. As shown in Fig. 15, after scaling the simulation amplitude, and for a lead break at the center of the panel, the scaled simulation response and the test response compare closely.

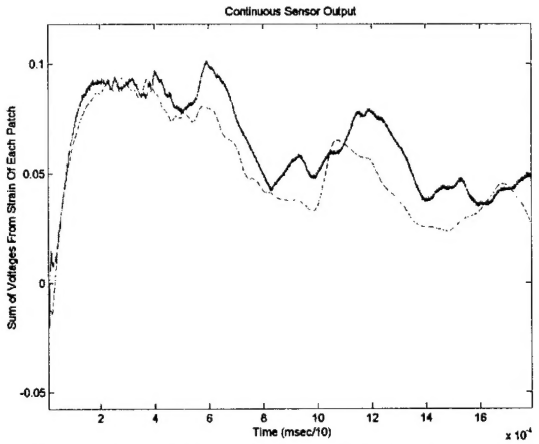

Figure 15. Response of the neural sensor due to a lead break (scaled simulation is dashed, test is solid line).

4. CONCLUSIONS

In this paper we discussed piezoceramic materials and their use as sensors and actuators in structures. The use of piezoceramic materials for structural condition monitoring was highlighted as an important application for smart materials. We discussed the concept of an Artificial Neural System (ANS) built using piezoceramic materials, microelectronics, and special signal processing algorithms. The ANS would be attached or integrated within structures in a highly dense spatial pattern to measure dynamic strains and acoustic waves. These measurements are interpreted to indicate if the structure is operating within the limits of its design specifications, and if there is any damage occurring to the structure. The innovation and novelty of this approach is that we are developing a biologically inspired highly distributed sensor that is potentially simpler, less expensive, less intrusive, and more sensitive than existing sensor technology. The neural system also represents the evolution of sensor technology from the macro-scale size to the micro-scale size. The small size of the sensor nerves combined with the large spatial coverage and simultaneous sensing from multiple branches or dendrites will provide the sensitivity to detect initiating damage in structures and this may revolutionize maintenance procedures and improve the safety of structures.

ACKNOWLEDGEMENT

The instrumentation used in the research in this

paper was partly provided by the Air Force Research Laboratory under agreement number F49620-00-1-0232. The U.S. government is authorized to reproduce and distribute reprints for governmental purposes notwithstanding any copyright notation thereon. This material is also based on research sponsored by the NSF Center for Advanced Materials and Smart Structures at NCA&TSU, the U.S. Army Research Office under contract/grant number G DAAD 19-00-1-0536, and the NASA Marshall Space Flight Center under grant number NAG8-1646. The support for this research is gratefully acknowledged.

REFERENCES

1. Cady W.G., "*Piezoelectricity: an introduction to the theory and applications of electromechanical phenomenon in crystals.*" (Dover Publications, New York, 1964).
2. Lines M.E. and Glass A.M., *Principles and Applications of Ferroelectric and related Materials* (Clarendon Press, Oxford, 1977).
3. Burns G, *Solid State Physics* (Academic Press, New York, 1985) Pg. 545.
4. Devonshire A.F., Phil Mag. 40 (1949) 1040.
5. Devonshire A.F., Adv. Phys. 3 (1954) 85.
6. Devonshire A.F., Phil. Mag. 42 (1961) 1065.
7. Cochran W., Adv. Phys. 9 (1960) 387.
8. Cochran W., Adv. Phys. 10 (1961) 401.
9. Cochran W., Adv. Phys. 18 (1969) 157.
10. Lines M.E., Phys. Rev. 177 (1969) 797, 812, 819.
11. Matthias B.T., Science 113 (1951) 591.
12. Bruce A.D. and Cowley R.A., J. Phys. C 6 (1973) 2422.
13. Migoni R., Bilz H and Bauerle, Phys. Rev. Lett 37 (1976) 1155.
14. Uchino K., *Piezoelectric Actuators and Ultrasonic Motors* (Kluwer Academic Publishers, Boston).
15. Francombe M.H., in *Physics of Thin Films: Mechanic and Dielectric properties*, ed: M.H. Francombe & J.L. Vossen (Academic Press, Boston, 1993) Vol. 21, p 225.
16. Auciello O., Kingon A.I. and Krupanidhi S.B., MRS Bulletin 21 (1996) 25.
17. Dey S.K. and Alluri P.V., MRS Bulletin 21 (1996) 44.
18. Polla D.L. and Francis L.F., MRS Bulletin 21 (1996) 59.
19. Ohring M., *The Materials Science of Thin Films* (Academic Press, Boston, 1992).
20. Yano Y. *et al.*, J. Appl. Phys. 76 (1994) 7853.
21. Chang L.L. *et al.*, J. Vac. Sci. Tech. 10 (1973) 655
22. Kern W. and Ban V.S., in *Thin Film Processes*, ed: J.L. Vossen and W. Kern (Academic Press, New York, 1978) p 256.
23. Tuttle B.A. and Schwartz, MRS Bulletin 21 (1996) 49.
24. Chopra K.L., Kainthla R.C., Pandya D.K. and Thakoor A.P., in *Physics of Thin Films*, ed: G. Hass, M.H. Francombe & J.L. Vossen (Academic Press, Paris, 1982) Vol. 12 p 168.
25. Auciello O. and Ramesh R., MRS Bulletin 21 (1996) 21.
26. Auciello O. and Ramesh R., MRS Bulletin 21 (1996) 31.
27. Hubler G., MRS Bulletin 16 (1992) 27.
28. Bent, A. A., Hagood, N. W., "Piezoelectric Fiber Composites with Interdigitated Electrodes," *J. of Intelligent Material Systems and Structures*, 8, 1998.
29. Continuum Control Corporation, 45 Manning Park, Billerica, MA 01821.
30. CeraNova Corporation, 101 Constitution Boulevard, Suite D, Franklin, MA 02038-2587.
31. Wilkie, Keats, NASA LaRC Macro-Fiber Composite Actuator, NASA news release, September 19, 00.
32. Muralt, P., Ferroelectric thin films for micro-sensors and actuators: a review, J. Micromech. Mircoeng., 10(2000), p. 136-146.
33. Jaffe, B., Cook, Jr., W.R., Piezoelectric Ceramics, Academic Press, 1971.
34. Wang, C., Chang, F., *Diagnosis of Impact Damage in Composite Structures with Built-In Piezoelectrics Network*, Proceedings of the SPIE, Vol. 3990, p. 13, 2000.
35. Schwarz, W.G., Read, M.E., Kremer, N.J. Hinders, M.K., Smith, B.D., *Lamb Wave Tomographic Imaging system for Aircraft Structural Health Assessment,* SPIE Conference on NDE of Aging Aircraft, Airports, and Aerospace Hardware III, Vol. 3586, p. 292, Newport Beach, CA, 1999.
36. Sundaresan, M.J., Ghoshal, A., and Schulz, M.J., "*Sensor Array System*," patent application, 6/00.
37. Sundaresan, M.J., Schulz, M.J., Ghoshal, A., Pratap, P., *"A Neural System for Structural Health Monitoring,"* SPIE 8th international Symposium on Smart Materials and Structures, March 4-8, 2001.
38. Zigmond, M.J., Boom, F., Landis, S.C., Roberts, J.L., Squire, L.R., Fundamental Neuroscience, Acacemic Press.
39. Ghoshal, A., Martin, W. N., Sundaresan, M. J., Schulz M. J., and Ferguson, F., *"Wave Propagation and Sensing in Plates,"* Third Workshop on Structural Health Monitoring, Stanford, CA, September 12-14, 2001.
40. William N. Martin Jr., Anindya Ghoshal, Gary Lebby, Mannur J. Sundaresan, Mark J. Schulz, Promod R. Pratap, *"Artificial Nerves for Structural Health Monitoring,"* Third Workshop on Structural Health Monitoring, Stanford, CA, Sept. 12-14, 01.
41. Schulz, M. J. Sundaresan, M.J., Ghoshal, A., Martin, W.N., *"Evaluation of Distributed Sensors for Structural Health Monitoring,"* abstract submitted, ASME Conference, Pittsburgh, PA, 2001.
42. Sundaresan, M.J., Schulz, M.J., Ghoshal, A., Pratap, P., *"A Neural System for Structural Health Monitoring,"* SPIE 8th international Symposium on Smart Materials and Structures, March 4-8, 2001.
43. Sundaresan, M. J. Schulz, M.J., Ghoshal, A. Ferguson, F., "*Active Fiber Composite Sensors and Actuators*," ACUN-3 International Composites Meeting, Technology Convergence in Composites Applications, Univ. of New South Wales, Sydney, Australia, February 6-9, 2001.
44. Endevco Corporation, San Juan Capistrano, CA.